21 CM OBSERVATIONS OF NGC 55

By B. J. Robinson* and K. J. van Damme*

[*Manuscript received August* 31, 1965]

Summary

Observations of the irregular galaxy NGC 55 have been made at a wavelength of 21 cm using the 210 ft radio telescope at Parkes. Line profiles have been measured for a grid of 60 points spaced at intervals of 6 min of arc. The mass of neutral hydrogen in the system is $2 \cdot 0 \times 10^9 M_\odot$, assuming a distance of $1 \cdot 74$ Mpc. The peaks of the profiles delineate a well-defined rotation curve, from which the total mass is found to be $2 \cdot 5 \times 10^{10} M_\odot$. The centroid of the hydrogen distribution and the centre of rotational symmetry are both displaced by about 3 min of arc from the nucleus of the system.

I. Introduction

Radio observations from the northern hemisphere (see, for example, Volders and van de Hulst 1959) have yielded detailed information on the hydrogen content and dynamics of six of the largest external galaxies, and hydrogen masses for a score more. Apart from the Magellanic Clouds (Kerr, Hindman, and Robinson 1954; Hindman, Kerr, and McGee 1963), measurements of the neutral hydrogen distribution and motions in southern galaxies have been hampered by the lack of a radio telescope with sufficient resolving power and a receiver of adequate sensitivity. Using a maser radiometer, Epstein (1964*a*) has measured the 21 cm line profile, averaged over a 53′ beam, for a few of the brighter galaxies as far south as declination $-40°$, and has attempted to determine rotation curves for them.

The construction of the 210 ft radio telescope at Parkes promised a considerable extension of the study of external galaxies, many of which can be easily resolved with the $13' \cdot 5$ beam at 21 cm wavelength. The telescope has been equipped with a low-noise parametric receiver (Robinson 1963), which is tunable over a wide band to measure the line radiation from galaxies with large red shifts.

The present paper is the first of a number of papers describing 21 cm investigations of southern galaxies, and contains a description of the receiving equipment and the methods of observation and reduction.

One of the first galaxies selected for study was NGC 55, a large, edge-on irregular system with optical isophotes that can be traced along the major axis out to half a degree from the centre (de Vaucouleurs 1961). Line profiles have been determined for a grid of 60 points spaced at intervals of 6 min of arc. Integration of the profiles allows the mass of hydrogen in the system to be determined. The radial velocities of the peaks of the profiles are displaced by the rotation of the system, and so a rotation curve can be constructed. The total mass and the mass distribution can then be estimated.

* Division of Radiophysics, CSIRO, University Grounds, Chippendale, N.S.W.

II. Receiving Equipment

With the dipole feed used on the 210 ft telescope, the beam at 21 cm was circular and $13' \cdot 5$ wide at half power. The response in the near sidelobes was more than 20 dB below the main beam, and thus caused no confusion in the observations. The antenna pattern, determined from observations of the radio source 3C353 (angular size $3' \cdot 5$) at different position angles, is shown by the continuous curve in Figure 1. The pattern is close to Gaussian in shape, and may be approximated

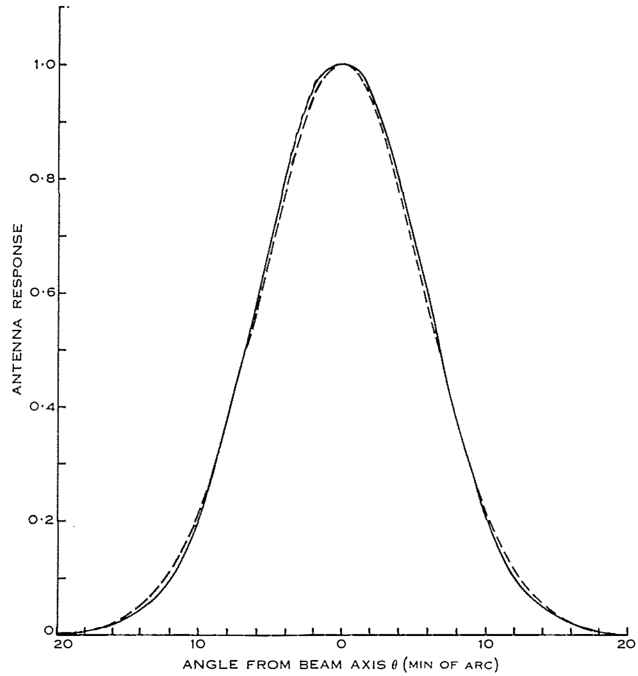

Fig. 1.—Measured antenna response $A(\theta)/A_0$ (continuous curve). The dashed line shows the function $f(\theta) = \exp -(\theta/11 \cdot 5)^2$.

by $f(\theta) = \exp -(\theta/11 \cdot 5)^2$, with θ, the angle from the beam axis, in minutes of arc; this function is shown by the dashed curve in Figure 1. The accuracy of the telescope pointing is believed to be better than ± 1 min of arc.

The receiver incorporates a two-stage parametric amplifier for low-noise performance, and frequency switching to eliminate response to continuum radiation and to minimize the effect of receiver instabilities. The frequency is switched by changing the pump frequency of a parametric up-converter (Robinson 1963) at the input, as shown schematically in Figure 2. The converter offers high stability at the expense of low gain, and has an output frequency of 2400 Mc/s, which is amplified by a fixed-frequency degenerate parametric amplifier (Robinson and de Jager 1962). The gain of the degenerate amplifier is carefully stabilized. Because of the folding of the spectrum that takes place in the degenerate amplifier, only one narrow-band filter is used, selecting a band centred exactly on 2400 Mc/s. The signal frequency is tuned by varying one of the pump oscillators of the up-converter. The remainder of the receiver is of conventional design.

The r.m.s. noise fluctuation at the output is equivalent to a change in the antenna temperature T_a of

$$\Delta T_a = \pi(T_n+T_a)/(B\tau)^{\frac{1}{2}},$$

where T_n is the receiver noise temperature, B is the pre-detector bandwidth, and τ is the time constant of the output integrator, assumed to be a simple RC circuit.

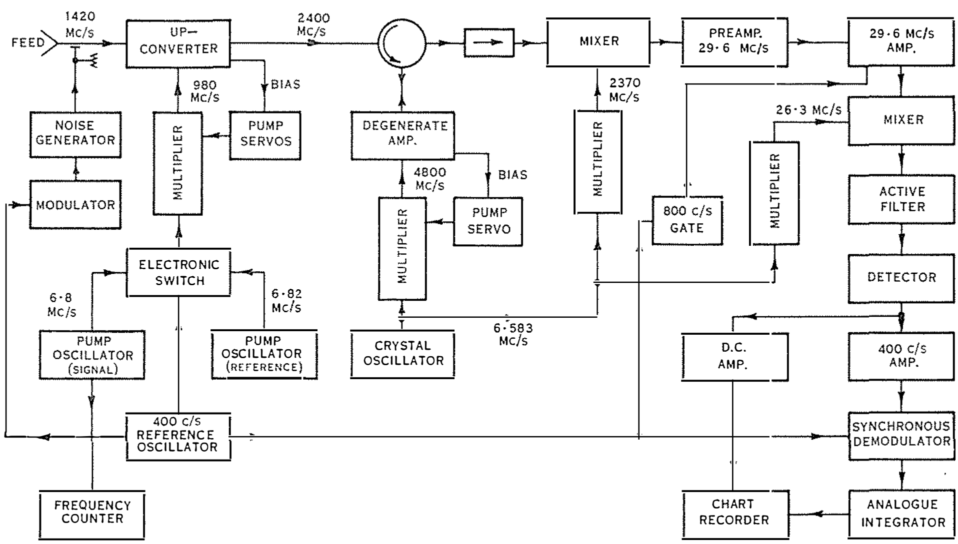

Fig. 2.—Schematic diagram of dual-parametric receiver with frequency switching.

For the measurements on NGC 55 we had $(T_n+T_a) = 170°$K, $B = 140$ kc/s, and $\tau = 15$ s, giving an r.m.s. noise fluctuation of 0·35 degK. Integration of the records by eye allowed measurements to be made with an accuracy of $\pm 0 \cdot 15$ degK. With the reference frequency 3 Mc/s below the signal frequency, drifts of the receiver output could be held to 0·1 degK/hr.

The frequencies were measured with an electronic counter having an accuracy of one part in 10^7. The drift of the variable oscillators generating the up-converter pump frequencies was about one part in 10^6 per hour. The other pump and local oscillators were controlled by a common quartz crystal oscillator, as shown in Figure 2.

The receiver sensitivity was calibrated frequently by injecting noise at the input from an argon discharge tube modulated in synchronism with the phase-sensitive detector. The level of the injected noise was calibrated at intervals by observing the continuum source 3C353, to establish an absolute scale of flux (see

Section V). The radiation from 3C353 is 3% polarized at 21 cm, so all calibrations were made at approximately the same hour angle.

III. Observations

Observations of NGC 55 were made to determine a sufficient number of 21 cm line profiles to deduce the motions and mass of the hydrogen in the galaxy. Scans were made in right ascension, at intervals of 6′ in declination, with a constant signal frequency. From a series of scans at frequencies spaced by one bandwidth (equivalent to 30 km/s in radial velocity), line profiles were constructed for a grid of points along lines parallel to the minor axis. Some intermediate scans were also made, such as that at $\delta = -39°32'$ shown in Figure 3. All the measurements were referred to a reference point at R.A. $00^h 09^m 36^s$, Dec. $-39°30'$. The observations were begun in November 1962, and were continued at intervals in January, June, and August 1963. The total telescope time involved was about 80 hr.

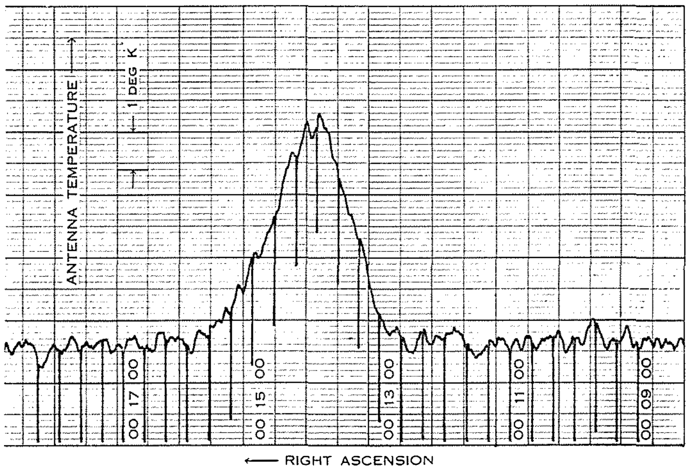

Fig. 3.—Right ascension scan across NGC 55 at declination −39°28′ (1962) at $\frac{1}{8}$°/min. The receiver was tuned to a frequency corresponding to a red shift of +180 km/s (bandwidth 140 kc/s, time constant 15 s).

The grid of profiles is shown in Figures 4(*a*) and 4(*b*), the radial velocities being referred to the Sun. Radiation is detected out to 38′ from the centre along the major axis, and for 18′ along the minor axis. The highest antenna temperatures are observed on the south-following side of the system, the observed radiation extending further in that direction than on the north-preceding side.

The displacement in radial velocity and the asymmetry of the profiles clearly reveal the rotation of the system. A special series of measurements was made to determine line profiles at points separated by 8′ along the major axis; the interval in radial velocity was reduced to 15 km/s so that the maxima of the profiles could be clearly delineated. The major-axis profiles are shown in Figure 5. The radial

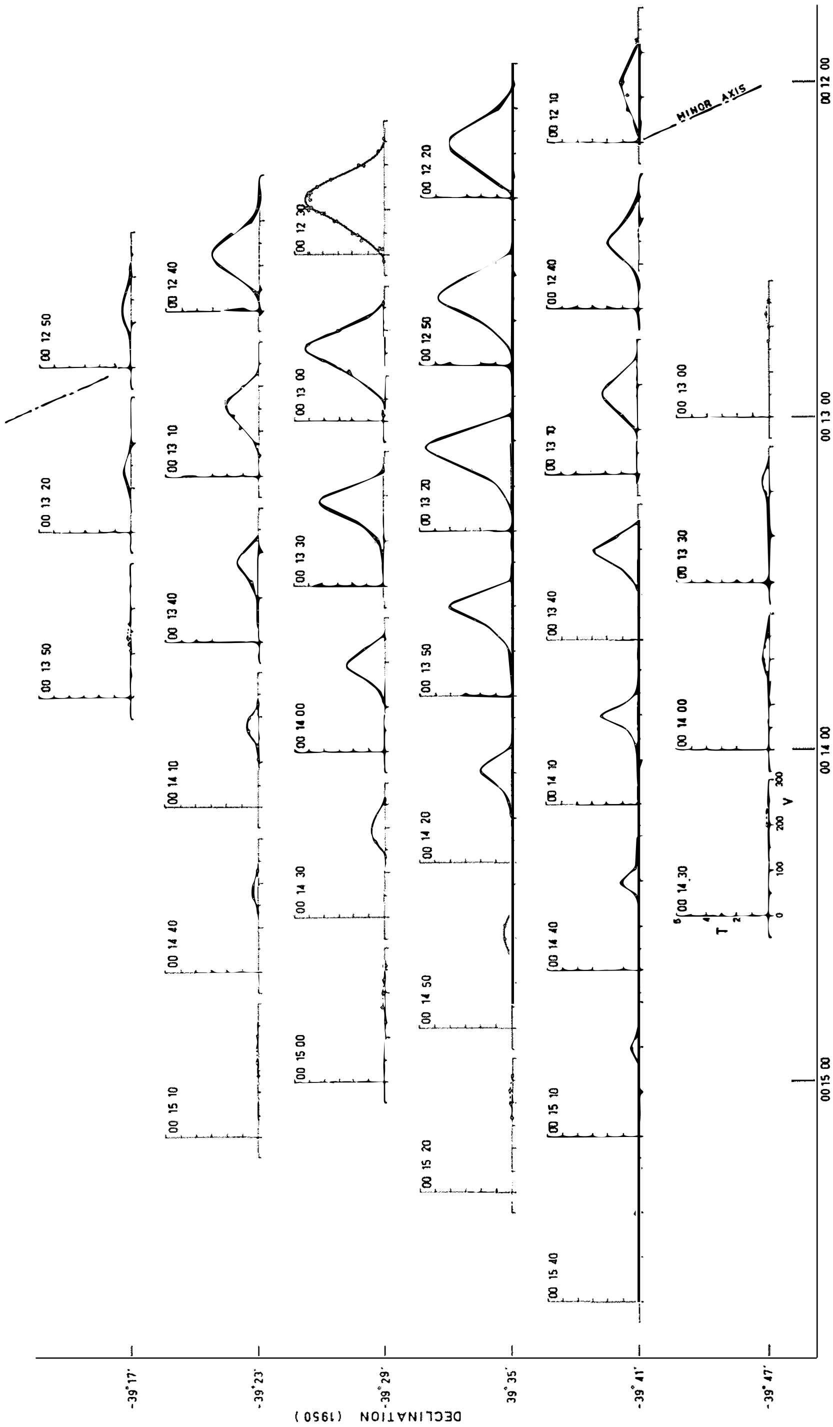

Fig. 4(a).—Grid of line profiles on the south-following side of NGC 55. The scale of antenna temperature T (°K) and velocity V (km/s) are marked on the profile at R.A. $00^h\,14^m\,30^s$, Dec. $-39°47'$.

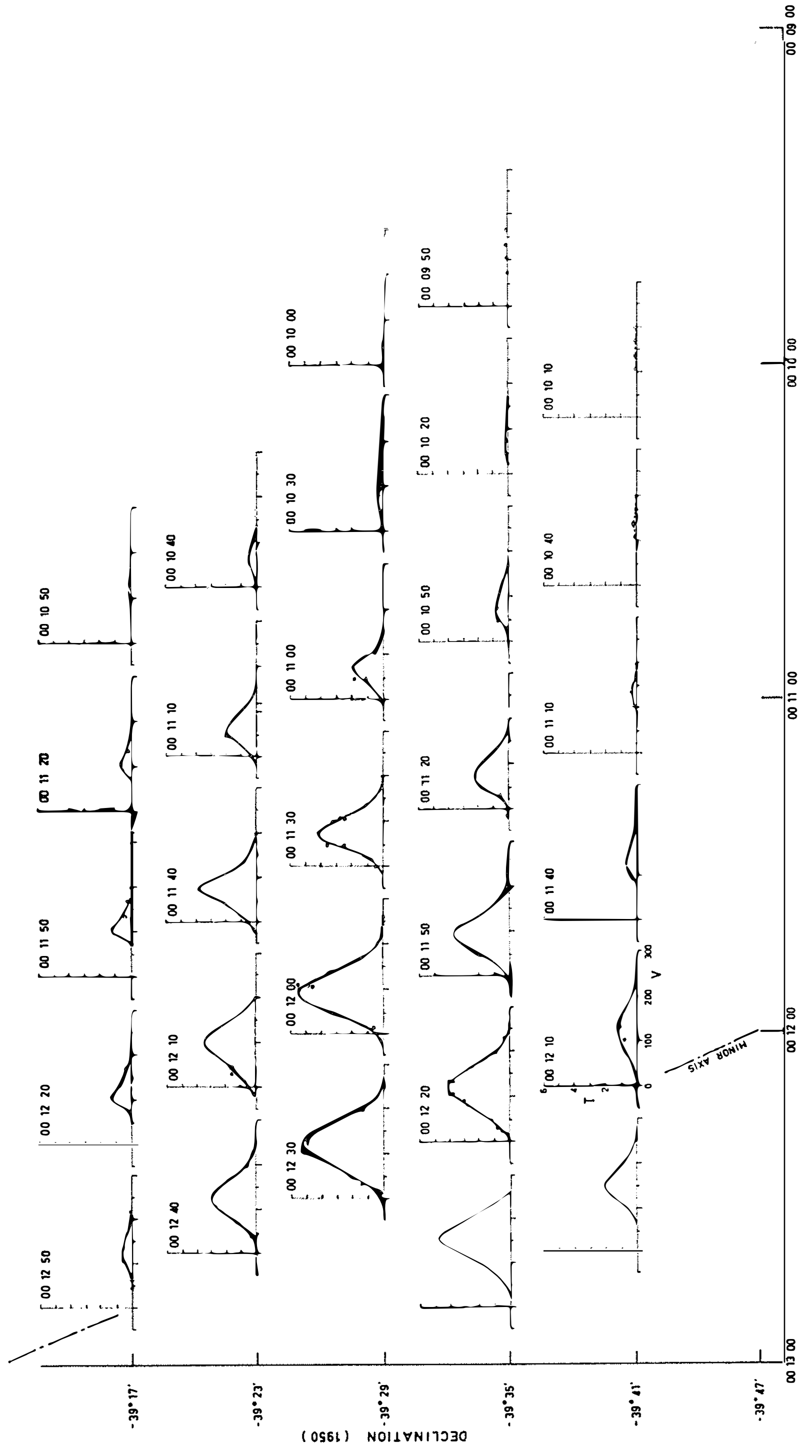

Fig. 4(*b*).—Grid of line profiles on the north-preceding side of NGC 55. The profiles along the minor axis are repeated from Figure 4(*a*).

21 CM OBSERVATIONS OF NGC 55

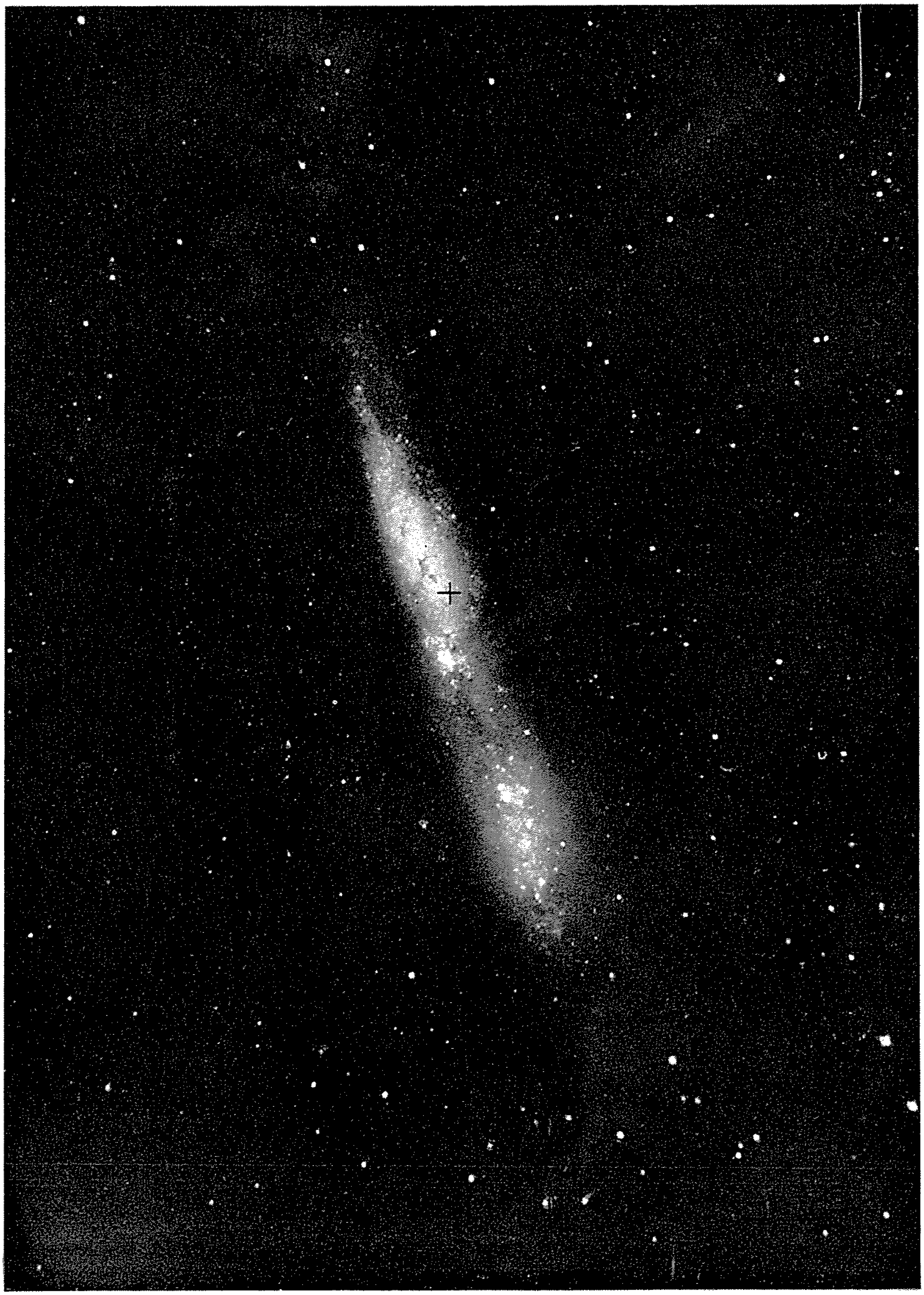

Mt. Stromlo 74 in. photograph of NGC 55 (scale 15″ per mm). North is at top, east at left. The NGC position is marked by a cross.

velocity of the profile peak changes from +55 to +205 km/s at points 32′ each side of the NGC position.

IV. Optical Characteristics of NGC 55

A photometric and spectroscopic study of NGC 55 has been made by de Vaucouleurs (1961). He classified the system as a "late-type, asymmetrical barred spiral similar to the Large Magellanic Cloud, seen edgewise and with the bar nearly along the line of sight". A recent 74 in. photograph,* reproduced in Plate 1, clearly

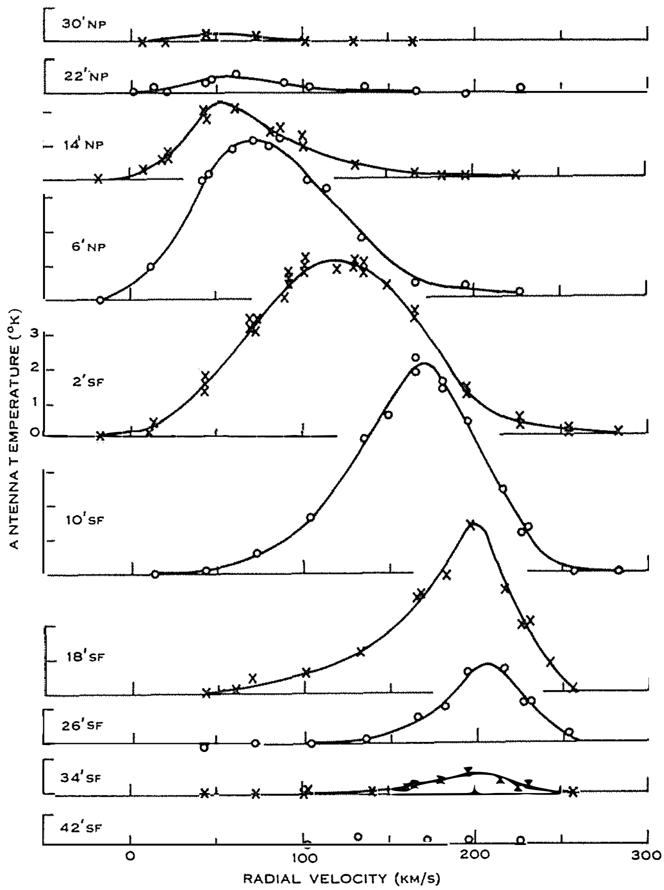

Fig. 5.—Line profiles measured at points along the major axis of NGC 55. The distance of each point from the nucleus is indicated; NP = north-preceding, SF = south-following.

shows the end of the "bar" and the fainter "arm" on the following side. The NGC position, located from the positions of stars on the plate, is marked by a cross; it is displaced 2′ east of the bright "nucleus". The main parameters of NGC 55 (from de Vaucouleurs 1961 and personal communication) are listed in Table 1.

* Kindly provided by Dr. A. R. Hogg.

V. Neutral Hydrogen Content

(a) *Relation of Hydrogen Content to Antenna Temperature*

When the optical depth τ is small, the number of hydrogen atoms N_{H} in a 1 cm^2 column in the line-of-sight is given by

$$N_{\mathrm{H}} = 3\cdot 87\times 10^{14}\int_0^\infty T_{\mathrm{b}}(\nu)\,\mathrm{d}\nu\,,$$

where $T_{\mathrm{b}}(\nu)$ is the brightness temperature of the element, a function of the frequency ν. Integrating over the projected image of the galaxy, we have

$$\iint N_{\mathrm{H}}\,\mathrm{d}\theta\,\mathrm{d}\phi = 3\cdot 87\times 10^{14}\iiint T_{\mathrm{b}}(\nu)\,\mathrm{d}\nu\,\mathrm{d}\theta\,\mathrm{d}\phi\,, \tag{1}$$

where θ and ϕ are angular coordinates.

Table 1

optical parameters of NGC 55

Parameter	Value	Parameter	Value
Type	SB(s)m	Distance (Mpc)	$1\cdot 74$
Right ascension (NGC, 1950)	$00^{\mathrm{h}}\,12^{\mathrm{m}}\cdot 5$	Total apparent magnitude (pg)	$7\cdot 9$
Declination (NGC, 1950)	$-39°30'$	Integrated luminosity (solar units)	$3\cdot 5\times 10^9$
Galactic longitude l^{II}	$332°45'$	Major-axis position angle*	107°
Galactic latitude b^{II}	$-75°43'$	Optical dimensions	$47'\times 9'$
Corrected distance modulus m_0-M	$26\cdot 2$	Equivalent linear dimensions (kpc)	$24\times 4\cdot 5$

* From Plate 1.

The brightness temperature is not an immediately observable quantity. The power received is proportional to the antenna temperature T_{a}, the average value of T_{b} weighted by the response of the telescope beam. For a beam direction (θ,ϕ) we have

$$T_{\mathrm{a}}(\theta\phi) = (1/\lambda^2)\iint A(\xi\eta)\,T_{\mathrm{b}}(\theta-\xi,\phi-\eta)\,\mathrm{d}\xi\,\mathrm{d}\eta\,, \tag{2}$$

where $A(\xi\eta)$ is the effective area of the antenna at an angle (ξ,η) to the principal axis of the beam. When the beam is scanned completely over the galaxy it can be shown that

$$\iint_{\mathrm{c}} T_{\mathrm{a}}(\theta\phi)\,\mathrm{d}\theta\,\mathrm{d}\phi = (1/\lambda^2)\iint_{\mathrm{gal}} T_{\mathrm{b}}(\theta\phi)\,\mathrm{d}\theta\,\mathrm{d}\phi\iint_{\mathrm{beam}} A(\xi\eta)\,\mathrm{d}\xi\,\mathrm{d}\eta\,, \tag{3}$$

where the integral of $T_{\mathrm{a}}(\theta\phi)$ extends over the region of the convolution of T_{b} and A. Substituting equation (3) in (1), we obtain

$$\iint_{\mathrm{gal}} N_{\mathrm{H}}\,\mathrm{d}\theta\,\mathrm{d}\phi = 3\cdot 87\times 10^{14}\lambda^2\Big\{\iiint_{\mathrm{c}} T_{\mathrm{a}}(\theta\phi\nu)\,\mathrm{d}\theta\,\mathrm{d}\phi\,\mathrm{d}\nu\Big\}\Big\{\iint_{\mathrm{beam}} A(\xi\eta)\,\mathrm{d}\xi\,\mathrm{d}\eta\Big\}^{-1}. \tag{4}$$

Following Seeger, Westerhout, and van de Hulst (1956), we can define a beam efficiency β such that

$$\iint_{\text{beam}} A(\xi\eta)\,\mathrm{d}\xi\,\mathrm{d}\eta = (1-\beta)\iint_{4\pi} A(\xi\eta)\,\mathrm{d}\xi\,\mathrm{d}\eta = (1-\beta)\lambda^2. \tag{5}$$

If x and y are linear coordinates on the projected image of the galaxy (in cm) and D is the distance (in kpc), we then have

$$\iint N_{\mathrm{H}}\,\mathrm{d}x\,\mathrm{d}y = 3\cdot 68\times 10^{57}D^2(1-\beta)^{-1}\iiint_{\mathrm{c}} T_{\mathrm{a}}(\theta\phi\nu)\,\mathrm{d}\theta\,\mathrm{d}\phi\,\mathrm{d}\nu\,,$$

so that the mass of hydrogen in the galaxy in solar masses is given by

$$M_{\mathrm{H}}/M_{\odot} = 3\cdot 10D^2(1-\beta)^{-1}\iiint_{\mathrm{c}} T_{\mathrm{a}}(\theta\phi\nu)\,\mathrm{d}\theta\,\mathrm{d}\phi\,\mathrm{d}\nu\,. \tag{6}$$

If we have a continuum source of known flux, we do not need a separate calibration of T_{a} and β. For a point source of flux S we have from equation (2)

$$T_{\mathrm{a}} = (A_0/\lambda^2)\iint T_{\mathrm{b}}(\theta\phi)\,\mathrm{d}\theta\,\mathrm{d}\phi = A_0\,.\,S/2k = (1-\beta)\lambda^2 S/2k\Omega'\,, \tag{7}$$

where A_0 is the effective area along the principal axis of the beam, k is the Boltzmann constant, and

$$\Omega' = \iint_{\text{beam}} \{A(\xi\eta)/A_0\}\,\mathrm{d}\xi\,\mathrm{d}\eta$$

is the effective solid angle of the beam. When S and Ω' are known, the scale of $T_{\mathrm{a}}/(1-\beta)$ can be determined. In these measurements the source 3C353 was used for calibration, the flux being taken as $(57\pm 3)\times 10^{-26}\,\mathrm{W\,m^{-2}\,(c/s)^{-1}}$. This value is based on the absolute flux of Cassiopeia A (Findlay, Hvatum, and Waltman 1965) and the ratio of the fluxes of 3C353 and Cassiopeia A measured by Goldstein (1962) and by Heeschen and Meredith (1961). From the antenna pattern of Figure 1, the effective solid angle of the main beam was found to be $\Omega' = 207$ sq min.

(*b*) *Results for NGC* 55

The usual method of determining the integral of T_{a} in equation (6) is to integrate the area under the line profiles in Figure 4. Contours of the integrated brightness $(1-\beta)^{-1}\int T_{\mathrm{a}}\,\mathrm{d}\nu$ for NGC 55 are shown in Figure 6. Planimeter integration of these contours yielded a value of $M_{\mathrm{H}} = 1\cdot 8\times 10^9\,M_{\odot}$ for an assumed distance of $1\cdot 74$ Mpc.

A more accurate method of finding M_{H} is to begin by determining $\int T_{\mathrm{a}}\,\mathrm{d}\alpha$ from integration of the original, unsmoothed right ascension (α) scans, and then to integrate over declination and frequency. This method gave $M_{\mathrm{H}} = 2\cdot 0\times 10^9\,M_{\odot}$ for the same distance of $1\cdot 74$ Mpc. One would expect the value of M_{H} to be higher than that determined by integrating the profiles, because integration of the original records would include the weak radiation in the outer regions; the profiles cannot be constructed reliably when the values of T_{a} become comparable with the receiver noise fluctuations. Taking the luminosity L of NGC 55 as $3\cdot 5\times 10^9\,L_{\odot}$, we have $M_{\mathrm{H}}/L = 0\cdot 57$.

Epstein (1964*a*) found that the hydrogen mass of NGC 55 was $1\cdot8\times10^9\ M_\odot$ at $D = 1\cdot74$ Mpc. However, he assumed that NGC 55 radiated at each frequency as a point source for the 53′ beam he used, so that M_H would be underestimated.

In deriving equation (6) we have assumed that the optical depth $\tau \ll 1$. Epstein (1964*b*) has computed the values of τ for model galaxies and shown that τ might be appreciable. For $M_H \approx 2\times10^9\ M_\odot$, Epstein's model would predict an average optical depth of $0\cdot6$ for NGC 55. This would make the true value of M_H a third greater than determined above.

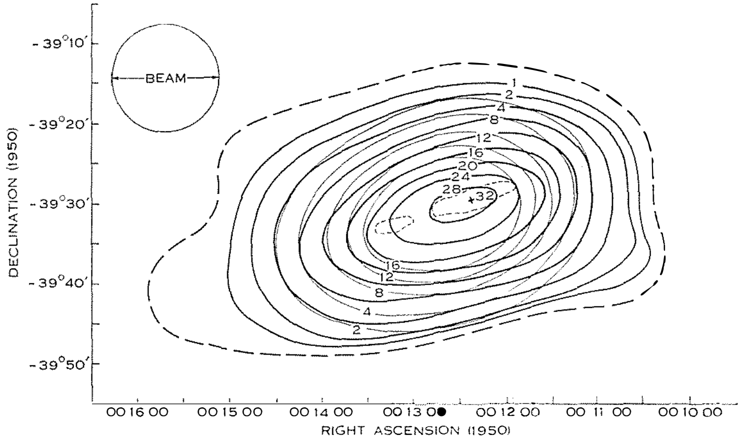

Fig. 6.—Contours of $(1-\beta)^{-1}\int T_a(\nu)\,d\nu$ for NGC 55 (heavy lines). Contour interval is 10^5 degK/s. The broken outer contour is the limit of radiation detected. The fine lines show some of the outer optical isophotes (normalized to the same central peak) when convolved with the 13′·5 beam. Dashed lines near the centre indicate the outline of the brightest parts of the galaxy.

The countours of integrated brightness in Figure 6 extend well beyond the main body of NGC 55, indicated schematically on the figure. To compare the distributions of stars and gas, the isophotes of de Vaucouleurs (1961) have been convolved numerically with the antenna beam pattern using the Silliac electronic computer of the University of Sydney. Some of the convolved isophotes are shown by the fine lines in Figure 6. Along the minor axis the contours correspond well, indicating similar distributions of gas and stars. Along the major axis the hydrogen contours extend further than the convolved isophotes, so that the gas distribution is wider, particularly on the south-following side.

The centroid of the neutral hydrogen distribution is at R.A. $= 00^h\,12^m\,35^s$, Dec. $= -39°31'$, a position displaced $2'\cdot5$ along the major axis to the south-following side of the bright nucleus. This corresponds to a distance of $1\cdot3$ kpc at the assumed distance of $1\cdot74$ Mpc. The HI centroid is thus displaced by a considerable distance from the centre of what de Vaucouleurs takes to be the bar of an SB(s)m system. However, the centroid of the outer optical isophotes is also displaced by 3′ from the nucleus in the same direction.

VI. Rotation Curve and Mass

(a) Observed Rotation Curve

For an edge-on system such as NGC 55, each line profile is an average of the radiation over the telescope beam and along each line-of-sight through the disk, smoothed by the finite receiver bandwidth. Approximately solid-body rotation occurs in the central regions, and there is no systematic variation of velocity along the line-of-sight (de Vaucouleurs 1961). Near or beyond the turnover point of the

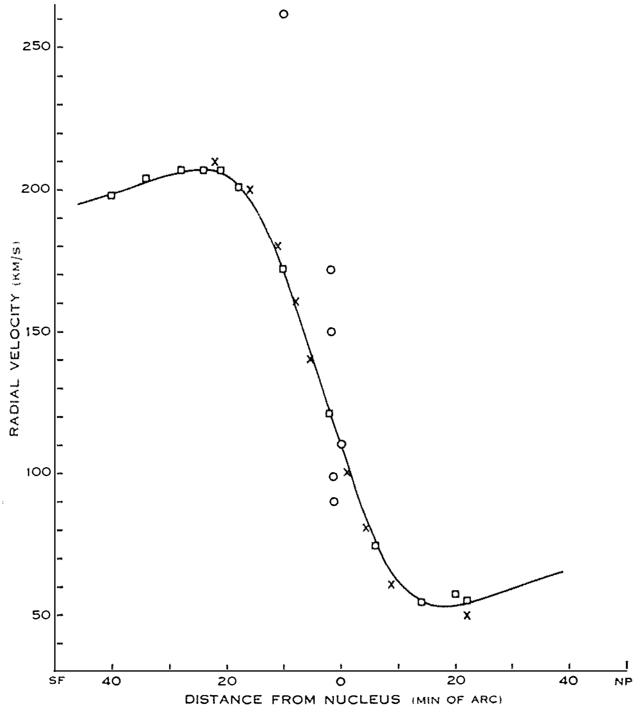

Fig. 7.—Observed radial velocities of profile peaks (□); velocities are reduced to the Sun. The continuous curve is the Bottlinger–Lohmann function. Open circles mark optical velocity measurements; crosses show the rotation curve corrected for Gaussian beam smoothing.

rotation curve the maximum velocity in each profile is that where the line-of-sight in the equatorial plane is normal to the radius vector, so that the profiles have the asymmetrical form seen in Figure 5. Without beam broadening the velocity of the peak of the profile would be close to the rotational velocity at that radius, the tail at greater velocities being produced by the random motions of the gas clouds and by the finite bandwidth. The shape of the observed profiles will be distorted because of the finite resolution of the 210 ft telescope, the rotational velocity derived from the peak being somewhat reduced. We shall later attempt to correct for the beam smoothing.

The velocities of the peaks of the major-axis profiles from Figures 4 and 5 are plotted in Figure 7 as a function of the distance from the nucleus. The centre of rotational symmetry is displaced by 3′ to the south-following side of the nucleus (close to the HI centroid), corresponding to a distance of 1·5 kpc. The high degree of symmetry about this displaced point can be seen from the continuous line in Figure 7, which is the theoretical rotation curve given by the Bottlinger–Lohmann function (Lohmann 1954).

The systemic velocity of the system, defined by the centre of symmetry of the rotation curve, is +130 km/s referred to the Sun. This should be compared with the Humason, Mayall, and Sandage (1956) value of the red shift of +210 ±50 km/s, referring to an emission patch 2′·7 preceding the nucleus. Velocities

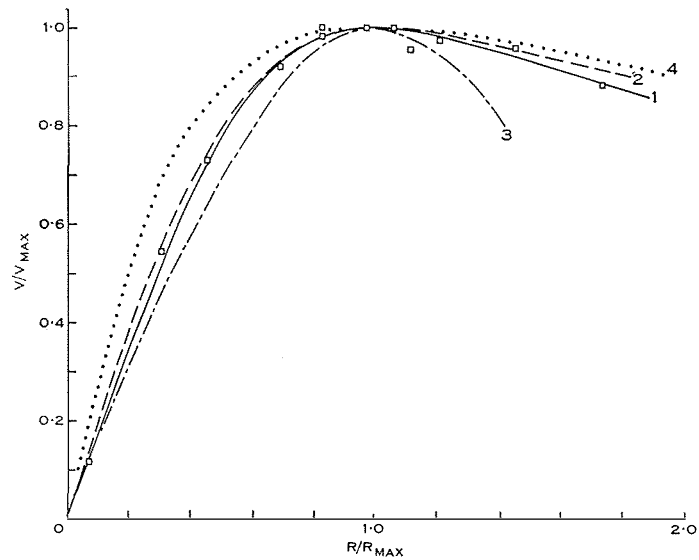

Fig. 8.—Normalized rotation curves. Measurements (□) for NGC 55 compared with (1) Bottlinger–Lohmann function, (2) Wyse and Mayall double-Gaussian model, (3) Perek oblate spheroid model for $n = 2$, and (4) Brandt function.

for several emission regions have also been measured by de Vaucouleurs (1961) and are shown by the open circles in Figure 7; they scatter rather widely about the radio rotation curve, probably indicating that the emission regions have large random velocities and lie at unknown points along the line-of-sight.

The measured rotation curve enables us to estimate the total mass of NGC 55. The measurements on the south-following side extend on to the start of the Keplerian branch, so that the mass derived from the outermost points will be a fair approximation to the total mass. If V is the velocity at a distance R from the rotation centre, the mass contained within a radius R is

$$M_{\mathrm{R}} = V^2 R/G,$$

where G is the gravitational constant $= 6\cdot 67 \times 10^{-8}$ dyn cm^2 g^{-2}. Taking $V =$ 69 km/s at $R = 36'$, we find that the mass inside this radius (18 kpc) is $2\cdot 0 \times 10^{10}\, M_{\odot}$.

An estimate of the total mass can be found from the fit of the Bottlinger–Lohmann rotation curve to the measurements. If R_M is the radius at which the maximum velocity V_M is found, the total mass of the system is then given by

$$M_T = 3V_M^2 R_M/2G.$$

The curve fitted to the measurements in Figure 7 has $V_M = 77$ km/s at $R_M = 21'$ (10·6 kpc), so that $M_T = 2\cdot 2\times 10^{10} M_\odot$.

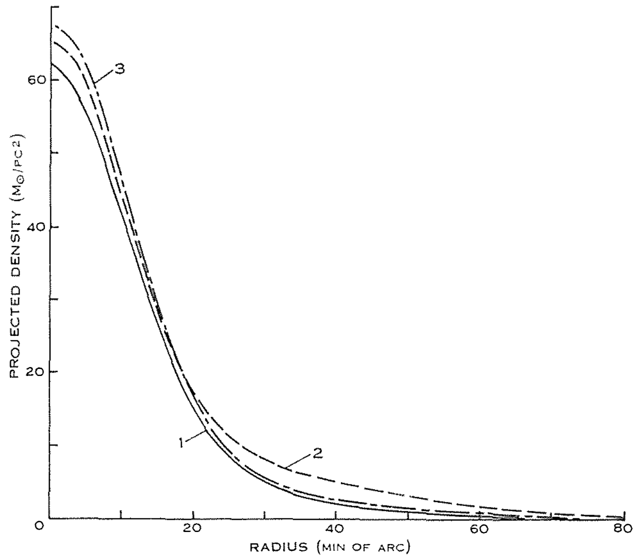

Fig. 9.—Projected density distributions for NGC 55, derived from observed rotation curve: (1) Bottlinger–Lohmann function, (2) Wyse and Mayall model. Curve 3 is a double-Gaussian model derived from the restored rotation curve.

It is possible to make a partial correction for the instrumental broadening and so obtain a better approximation to the true rotation curve. However, before this is attempted, we shall determine some mass distributions that would give rotation curves similar to the measured one. This will enable us to judge the magnitude of the errors introduced by the finite resolution.

In Figure 8 a number of theoretical rotation curves, normalized at the velocity maximum, are compared with the measurements (reflected about the centre of rotational symmetry). As well as for the Bottlinger–Lohmann function, a good fit is found for a Wyse and Mayall (1942) thin-disk model of two superimposed Gaussian distributions, one having a quarter of the density of, and extending three times beyond, the other. Also shown is the curve for Perek's (1948) oblate spheroid model (for $c/a = 0\cdot 14$ and $n = 2$) and the velocity function introduced by Brandt (1960); neither of the latter functions fits the measured curve. The density distributions corresponding to the first two theoretical curves are shown in Figure 9; for the Bottlinger–Lohmann function the density distribution has been computed by

Castleman (personal communication), following the methods of Brandt and Belton (1962). The two distributions differ markedly in the outer regions, reflecting the inability of the observations to define the rotation curve well beyond the velocity maximum. The total mass for the thin-disk model is $2 \cdot 6 \times 10^{10} M_{\odot}$. This is higher than the $2 \cdot 2 \times 10^{10} M_{\odot}$ for the Bottlinger–Lohmann curve, because of the contribution of the low density extension of the double-Gaussian model.

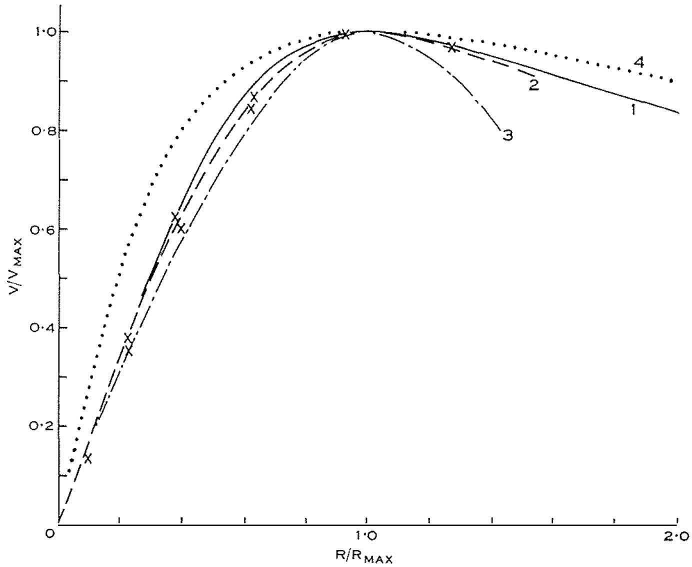

Fig. 10.—Normalized rotation curves. Restored points (×) for NGC 55 compared with (1) Bottlinger–Lohmann function, (2) Wyse and Mayall model, (3) Perek oblate spheroid model for $n = 2$, and (4) Brandt function.

(b) Rotation Curve corrected for Beam Broadening

Approximate methods for determining the "principal solution" for a brightness distribution smoothed by a finite antenna beam have been given by Bracewell (1955, 1956). However, the fine detail of the distribution is irretrievably lost. Kerr and de Vaucouleurs (1956) have modified the correction for a Gaussian beam to "restore" the velocity distributions for the Magellanic Clouds, although there is no formal justification for the modification. In principle, one could construct line profiles from restored maps of $T_a(V)$ at various fixed velocities, but the procedure would be laborious. To obtain the restored rotation curve we require to find only the velocities at which the restored profiles have their maxima. If we differentiate equation (2) with respect to velocity, we have

$$\partial T_a(\theta\phi V)/\partial V = (1/\lambda^2) \iint A(\xi\eta)\{\partial T_b(\theta-\xi, \phi-\eta, V)/\partial V\}\, d\xi\, d\eta .$$

Thus we find approximately where $\partial T_b/\partial V$ is zero by restoring the observed $\partial T_a/\partial V$. In the present case the beam shape is close to Gaussian (Fig. 1), and simple methods of correction can be used (Bracewell 1955).

TABLE 2

COMPARISON OF IRREGULAR GALAXIES

c is a correction factor to the assumed distance scale

Galaxy	Assumed Distance (Mpc)	M_H ($10^9 M_\odot$)	M_T ($10^{10} M_\odot$)	L_{pg} ($10^9 L_\odot$)	M_H/M_T	M_H/L	M_T/L	References*
NGC 55	$1\cdot74c$	$2\cdot0c^2$	$2\cdot5c$	$3\cdot5c^2$	$0\cdot08c$	0·57	$7\cdot2c^{-1}$	
LMC	0·052	0·8	1·5	3·2	0·054	0·25	4·8	1, 2, 6
SMC	0·063	0·5	0·33	0·6	0·15	0·83	5·5	1, 2, 5
NGC 6822	0·50	0·15	0·15	0·12	0·10	1·2	12	3
IC 1613	0·63	0·05	0·033	0·064	0·15	0·78	5·1	3
NGC 3109	2·2	1·7	0·8	0·8	0·21	2·1	10	8
NGC 4214	3·3	0·98	0·33	1·7	0·30	0·58	1·9	7
NGC 4449	3·3	2·4	2·1	2·1	0·11	1·1	10	7
NGC 4656	3·3	1·5	0·8	0·98	0·19	1·5	8	7
Holmberg II	3·3	2·0	0·96	0·82	0·21	2·4	12	7
Sextans A	2·0	0·28	0·27	0·19	0·10	1·5	14	7
IC 10	1·0	0·2	—	0·14	—	1·4	—	4

* References to measurements are:

1. Kerr, Hindman, and Robinson (1954),
2. Kerr and de Vaucouleurs (1956),
3. Volders and Hogbom (1961),
4. Roberts (1962),
5. de Vaucouleurs (1962),
6. de Vaucouleurs and de Vaucouleurs (1963),
7. Epstein (1964*a*),
8. van Damme (1966).

The peak velocities obtained by restoring $\partial T_a/\partial V$ for the observed major-axis profiles are shown by the crosses in Figure 7. The restoration has increased the rotational velocities and moved the maxima closer to the centre of the system; the centre of rotational symmetry is not sensibly changed. The weakness of the outlying profiles makes the restoration process uncertain, and the corrected curve is not taken far beyond the velocity maximum. From the outermost point we can deduce that the mass inside a radius of 25′ is $1 \cdot 9 \times 10^{10}\, M_\odot$.

Several model velocity functions (normalized) are compared with the restored rotation curve in Figure 10. The best fit to the restored curve is a Wyse and Mayall thin-disk model comprising two Gaussian density distributions, one having a tenth of the density of the other and extending three times further. This distribution is shown by curve 3 in Figure 9. The total mass of the model comes to $2 \cdot 2 \times 10^{10}\, M_\odot$.

The models considered above have negligible thickness and underestimate the mass of the system. For a galaxy with an axial ratio of 1/5 the true mass can be as much as 20% greater than is found from the highly flattened models (Kerr and de Vaucouleurs 1956; Brandt 1960). We shall therefore adopt a value of $2 \cdot 5 \times 10^{10}\, M_\odot$ for the mass of NGC 55, which has an axial ratio close to 1/5.

For a mass M_T of $2 \cdot 5 \times 10^{10}\, M_\odot$, the hydrogen content of NGC 55 becomes $M_H/M_T = 0 \cdot 08$, while the mass–luminosity ratio M_T/L is $7 \cdot 2$.

VII. Comparison with Other Irregular Galaxies

Optically NGC 55 has been closely compared with the Large Magellanic Cloud (LMC) by de Vaucouleurs (1961). A résumé of the characteristics of the two systems found at 21 cm has been given previously (Robinson and van Damme 1964) and the major results (revised on the basis of additional measurements) are listed in Table 2. NGC 55 is nearly twice as massive as the LMC, and has three times the mass of neutral hydrogen. In NGC 55 the centroid of the hydrogen distribution is displaced by 1·3 kpc from the bright nucleus in the centre of the bar, while for the LMC the corresponding distance is 1·2 kpc. The centres of rotation are also displaced from the centre of the bar by 1·5 kpc in NGC 55 and 800 pc in the LMC. These results provide support for de Vaucouleurs' morphological comparison of the two systems.

Data for other irregular galaxies are included in Table 2. NGC 55, the LMC, and NGC 4449 stand out as more massive systems, and tend to have lower values of M_H/M_T and M_H/L than the smaller, less luminous, galaxies.

VIII. Conclusion

The 21 cm measurements have shown that the mass of hydrogen in NGC 55 is $2 \cdot 0 \times 10^9\, M_\odot$, the distribution of the gas being slightly more extended than that of the stars. The total mass deduced from the rotation of the system is $2 \cdot 5 \times 10^{10}\, M_\odot$, and an approximate mass distribution has been obtained. The hydrogen content and the hydrogen–luminosity ratio indicate that NGC 55 is of a type closely similar to the Large Magellanic Cloud, although more massive. Detailed morphological comparison of the two systems is supported by evidence for similar displacements from the centre of the bar of the centroids of the hydrogen and luminosity distributions and of the centre of rotation.

IX. Acknowledgments

The parametric receiver was constructed with the assistance of the staff of the Netherlands Foundation for Radio Astronomy and members of the CSIRO Radiophysics Laboratory. Observations were carried out with the help of the resident staff of the Australian National Radio Astronomy Observatory at Parkes. The excellent performance of the radio telescope was largely due to the efforts of Mr. A. J. Shimmins.

X. References

Bracewell, R. N. (1955).—*Aust. J. Phys.* **8**: 54.
Bracewell, R. N. (1956).—*Aust. J. Phys.* **9**: 297.
Brandt, J. C. (1960).—*Astrophys. J.* **131**: 293.
Brandt, J. C., and Belton, M. J. S. (1962).—*Astrophys. J.* **136**: 352.
van Damme, K. J. (1966).—*Aust. J. Phys.* (in press).
Epstein, E. E. (1964*a*).—*Astr. J.* **69**: 490.
Epstein, E. E. (1964*b*).—*Astr. J.* **69**: 521.
Findlay, J. W., Hvatum, H., and Waltman, W. B. (1965).—*Astrophys. J.* **141**: 873.
Goldstein, S. J. (1962).—*Astr. J.* **67**: 171.
Heeschen, D. S., and Meredith, B. L. (1961).—*Publ. Natl Radio Astr. Obs.* **1**: 121.
Hindman, J. V., Kerr, F. J., and McGee, R. X. (1963).—*Aust. J. Phys.* **16**: 570.
Humason, M. L., Mayall, N. U., and Sandage, A. R. (1956).—*Astr. J.* **61**: 97.
Kerr, F. J., Hindman, J. V., and Robinson, B. J. (1954).—*Aust. J. Phys.* **7**: 297.
Kerr, F. J., and de Vaucouleurs, G. (1956).—*Aust. J. Phys.* **9**: 90.
Lohmann, W. (1954).—*Z. Astrophys.* **35**: 159.
Perek, L. (1948).—*Contr. Astr. Inst. Masaryk Univ.* **1**: No. 6.
Roberts, M. S. (1962).—*Astr. J.* **67**: 431.
Robinson, B. J. (1963).—*Proc. Instn Radio Engrs Aust.* **24**: 119.
Robinson, B. J., and van Damme, K. J. (1964).—Symp. IAU–URSI No. 20 (Canberra 1963). pp. 276–8.
Robinson, B. J., and de Jager, J. T. (1962).—*Proc. Instn Elect. Engrs* **109**(B): 267.
Seeger, C. L., Westerhout, G., and van de Hulst, H. C. (1956).—*Bull. Astr. Insts Neth.* **13**: 89.
de Vaucouleurs, G. (1961).—*Astrophys. J.* **133**: 405.
de Vaucouleurs, G. (1962).—"Problems of Extra-galactic Research." (Ed. G. C. McVittie.) pp. 3–21. (Macmillan: New York.)
de Vaucouleurs, G., and de Vaucouleurs, A. (1963).—*Astrophys. J.* **137**: 374.
Volders, L., and Högbom, J. A. (1961).—*Bull. Astr. Insts Neth.* **15**: 307.
Volders, L., and van de Hulst, H. C. (1959).—Symp. IAU No. 9 (Paris 1958). pp. 423–30.
Wyse, A. B., and Mayall, N. U. (1942).—*Astrophys. J.* **95**: 24.